N88-14936

ANALYSIS AND PERFORMANCE PREDICTION OF SCRAMJET

INLETS UTILIZING A THREE-DIMENSIONAL

NAVIER-STOKES CODE

S_{10} - 07

117234

22 P.

Ajay Kumar and Carl A. Trexler
NASA Langley Research Center
Hampton, Virginia

PRECEDING PAGE BLANK NOT FILMED

PAGE 186 INTENTIONALLY BLANK

Scramjet inlets have high geometric complexity as well as a highly complex flow field. The flow is primarily three-dimensional, possibly turbulent. It involves complex shock and expansion wave interactions. It also involves strong shock/boundary-layer interactions resulting in separated regions. Further, due to the aft placement of the cowl, the internal flow ahead of the cowl is exposed to the external flow resulting in interaction between the two.

● PRIMARILY THREE-DIMENSIONAL, POSSIBLY TURBULENT

● INVOLVES COMPLEX SHOCK AND EXPANSION WAVE INTERACTIONS

● INVOLVES STRONG SHOCK/BOUNDARY-LAYER INTERACTIONS RESULTING IN SEPARATED REGIONS

● INVOLVES INTERACTION BETWEEN INTERNAL AND EXTERNAL FLOW FIELD RESULTING IN FLOW SPILLAGE
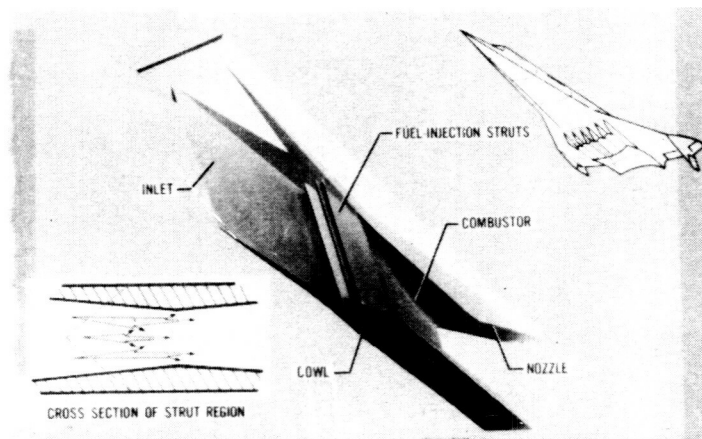
Due to the complex nature of the flow, most scramjet inlet research to date has been experimental with little supporting analytical work. However, with the increasing availability of high-speed, large-storage computers and advanced computing techniques, it has become feasible to numerically simulate flow fields associated with high-speed inlets. The goal of the present research is to provide an accurate and efficient inlet analysis tool that allows promising design configurations to be developed with less reliance on extensive wind-tunnel testing.

## 3-D EULER/NAVIER-STOKES INLET ANALYSIS CODE

The research to provide inlet analysis software started with the development of a two-dimensional Euler and Navier-Stokes code; this was followed by the three-dimensional Euler and Navier-Stokes code. An axisymmetric version of the code is also available. In this presentation, I will discuss only the three-dimensional analysis results. This figure briefly describes the features of the code.

- Governing equations in conservation form

- Boundary-fitted curvilinear coordinates

- Algebraic turbulence model

- MacCormack's explicit or explicit-implicit scheme

- Fully vectorized

Special attention has been given to organize the code for maximum use of the central core of the computer. The code is fully vectorized and calculations are performed in planes with temporary reusable vectors maintained only in two local planes. Further, to save on storage requirements, the transformation metric data are calculated in each time-step. On the CDC VPS 32 computer, the code can accommodate a maximum of 1.4×10^6 grid points without going out of primary memory of the system. It has a compute rate of about $.7 \times 10^{-5}$ sec per grid point per time step. For more details, see reference 1.

- The code is written in Star Fortran and uses 32-bit word arithmetic

- Transformation metric data are calculated in each time step

- Calculations are performed in planes with temporary reusable vectors maintained only in two local planes

Predictor step completed

Corrector step started
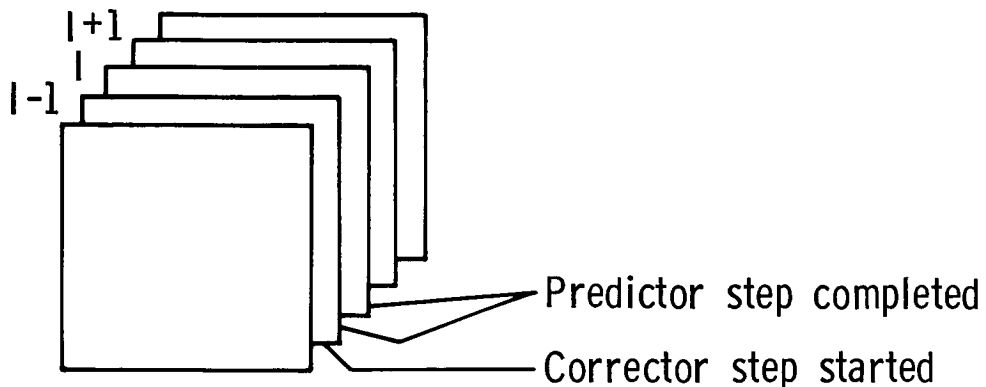
- Maximum grid size that can be used without going out of primary memory is approximately 1.4 million points

- Compute rate is $.7 \times 10^{-5}$ sec/grid point for one complete time-step (i.e. both predictor and corrector step)

- Typical solution can be obtained in 20-150 minutes CPU time for up to 100,000 grid points

SYMMETRIC WEDGE CORNER AND SCHEMATIC OF CORNER FLOW

To verify the code, calculations were made for laminar and turbulent flow for a 3-D symmetric wedge corner shown in the figure. The flow in such a corner is representative of the type of flow inside a scramjet inlet. A schematic of the basic characteristics of the corner flow is also presented in the figure. It has very complex structure that includes wall shocks, corner shock, internal shocks, and slip lines.

In the present analysis, a grid of 39 x 61 x 61 points is used with suitable refinement near the corner walls. Calculations are made for the following conditions:
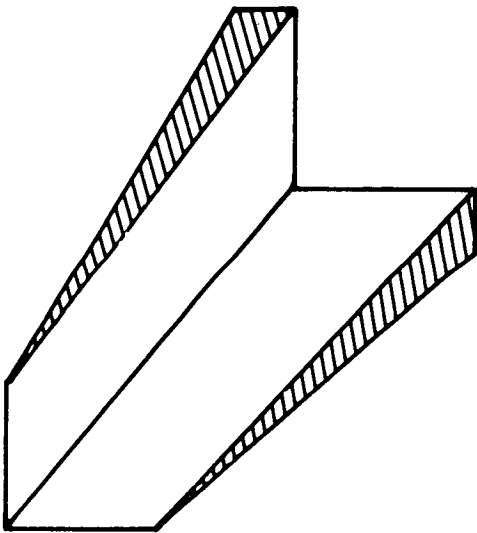
$$M_\infty = 3.0$$

$$N_{R_\infty} = 3.9 \times 10^5; \text{ laminar flow}$$
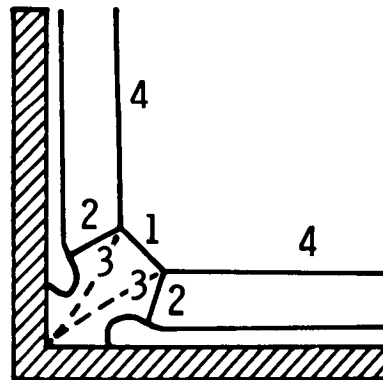
$$1.1 \times 10^6; \text{ turbulent flow}$$

$$T_\infty = 105°K$$

$$T_w = 294°K$$

1 CORNER SHOCK
2 INTERNAL SHOCK
3 SLIP LINE
4 WALL SHOCK

(a)

(b)

The figure shows the density contours for the laminar flow as obtained from the present code. Experimentally determined contours are also shown. It is seen that the calculations have predicted the corner flow features very well and are in very good agreement with the experiment.

LAMINAR FLOW

O EXPERIMENTAL RESULTS (Ref.2)

$$\frac{z - z_w}{x}$$

$$\frac{y - y_w}{x}$$
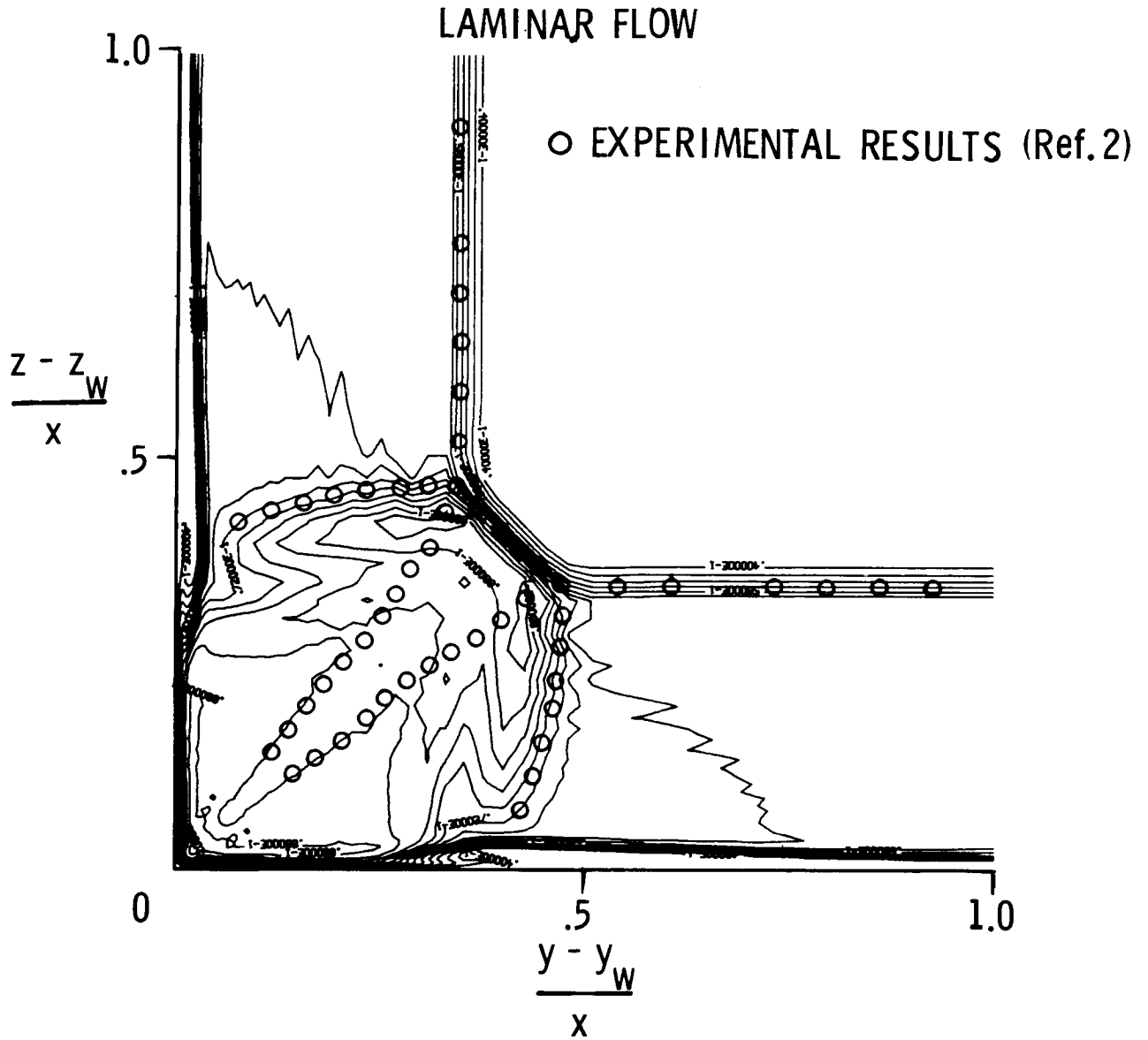
SURFACE PRESSURE DISTRIBUTION FOR SYMMETRIC WEDGE CORNER

This figure presents a comparison of the sidewall pressure distribution with experiment for the laminar and turbulent flow. The predicted results compare well with the experimental results.
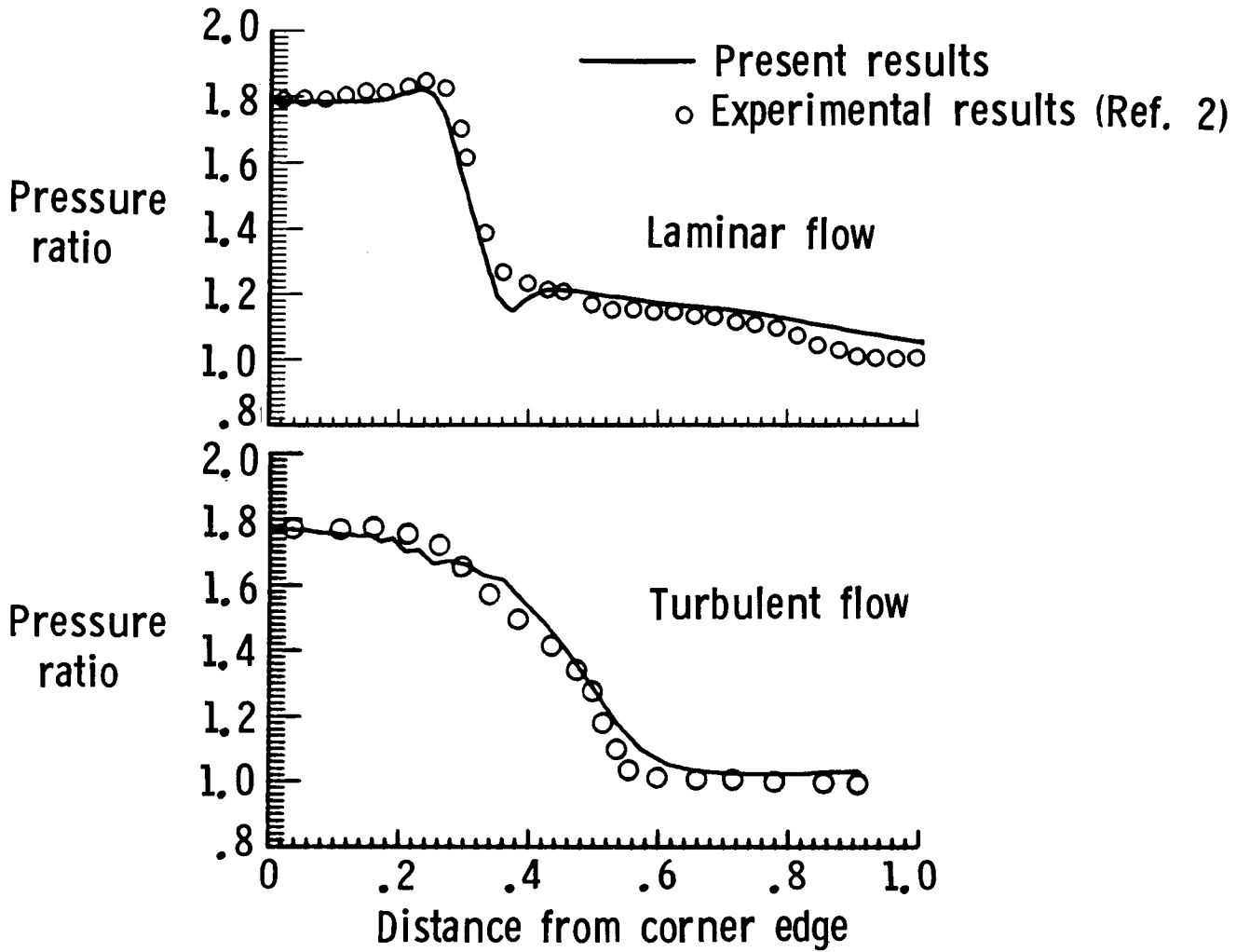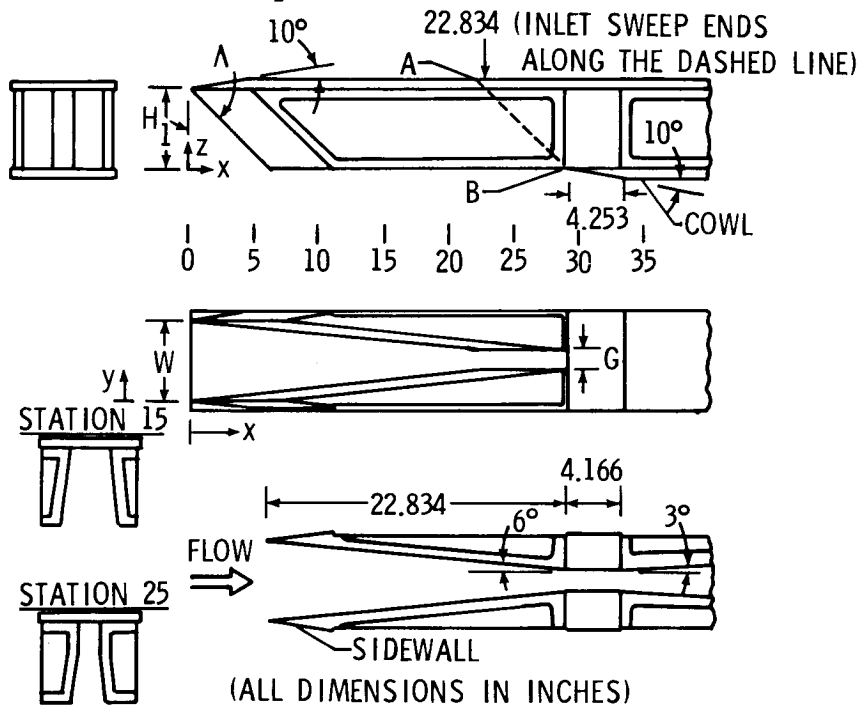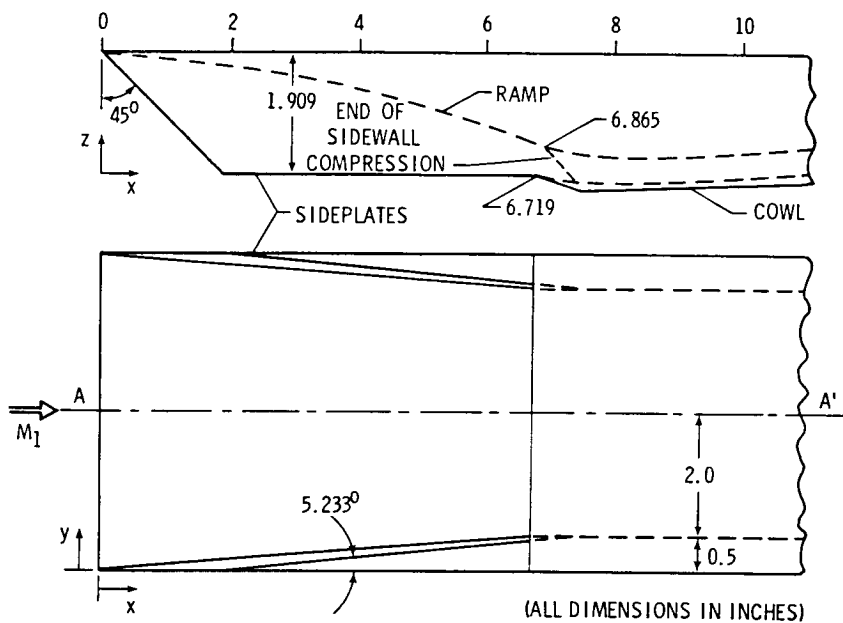
The next four figures present a variety of high-speed inlet configurations that have been analyzed with the 3-D Navier-Stokes code. Results on two other configurations will be presented later.
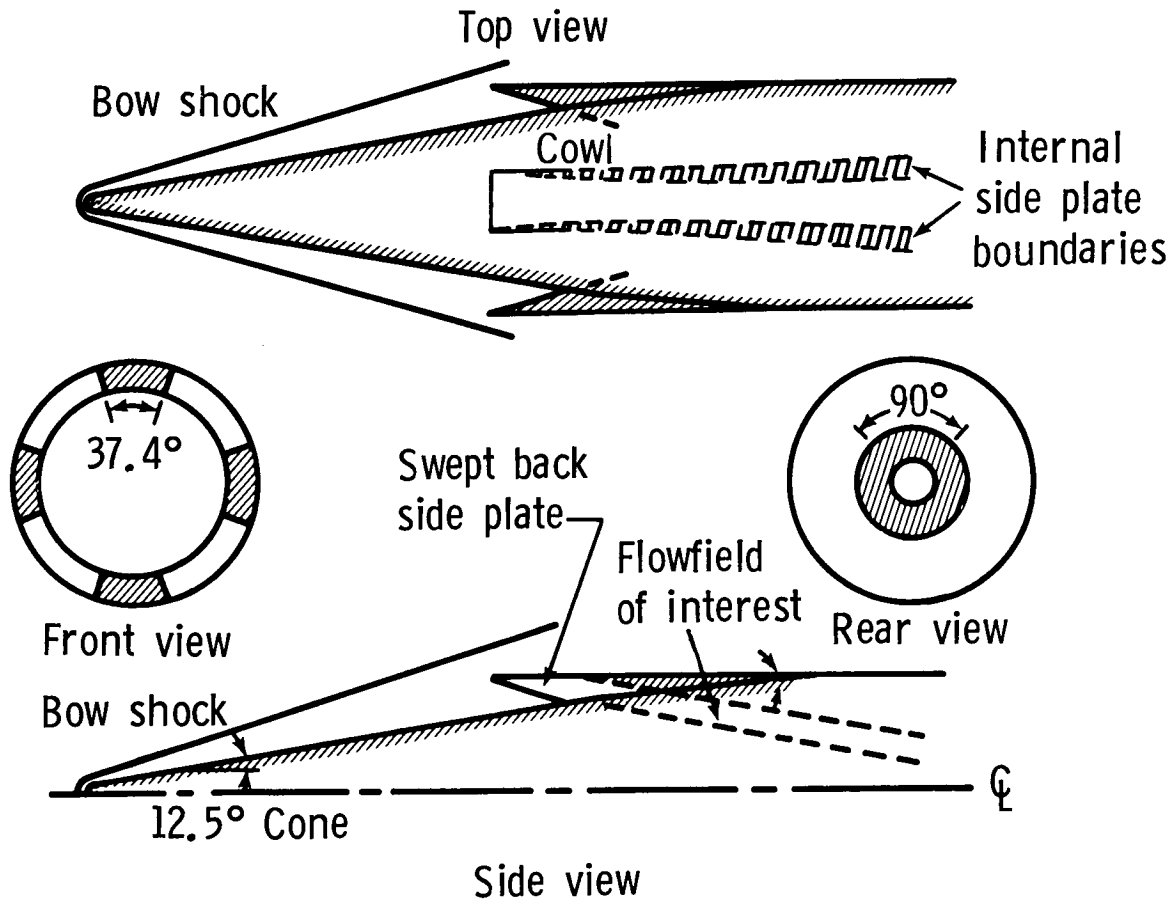
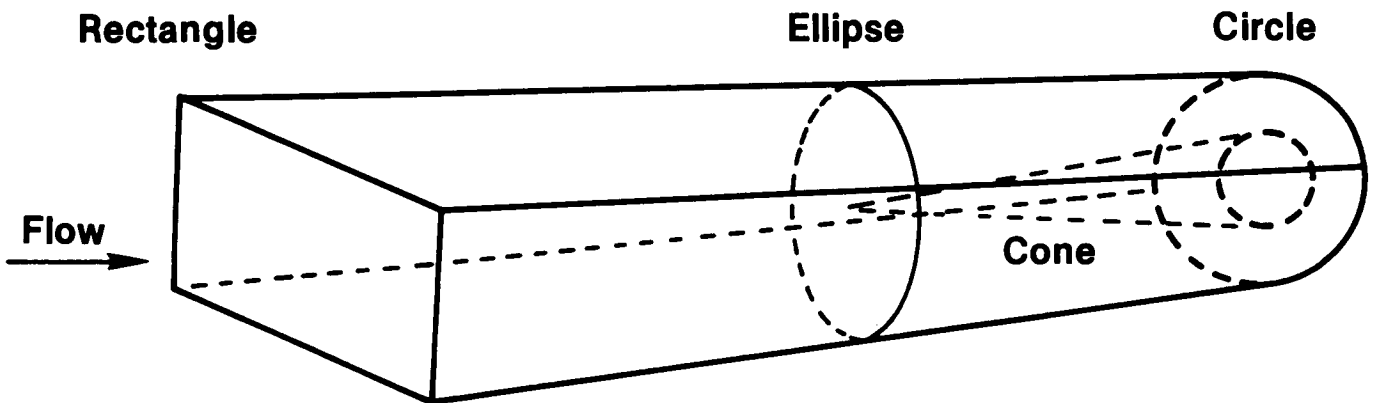## GEOMETRY OF THE PARAMETRIC SCRAMJET ENGINE
$H_1 = 7.2$, $W = 6.4$, $G = 1.6$

(ALL DIMENSIONS IN INCHES)

GEOMETRY OF AFT INLET CONFIGURATION

(ALL DIMENSIONS IN INCHES)

TYPICAL MITS INLET CONFIGURATION

Top view

Bow shock

Cowl

Internal
side plate
boundaries

37.4°

90°

Swept back
side plate

Flowfield
of interest

Front view

Rear view

Bow shock

12.5° Cone

C_L

Side view

SUPERSONIC INLET DUCT

Rectangle

Ellipse

Circle

Flow

Cone

PHYSICAL DOMAIN OF COMPUTATION

Before any results on the inlets are presented, a brief description is given on how the present analysis accounts for the interaction of internal flow with the external flow. As mentioned earlier, this interaction occurs due to the aft placement of the cowl, which exposes the flow inside the inlet to the flow outside the inlet in the region ahead of the cowl. In order to account for this interaction, a portion of the outside flow under the cowl plane must be included in the analysis. Ideally one should go down and around the sidewalls far enough so that the free-stream conditions can be applied on the free boundaries but this would greatly increase the computational requirements. In the present analysis, the region is extended as shown in the figure by the dashed line (only half of the flow is calculated due to symmetry). This limited extension of the computational domain should be sufficient because in the actual engine, several such modules will be placed side by side.

SYMMETRY
LINE
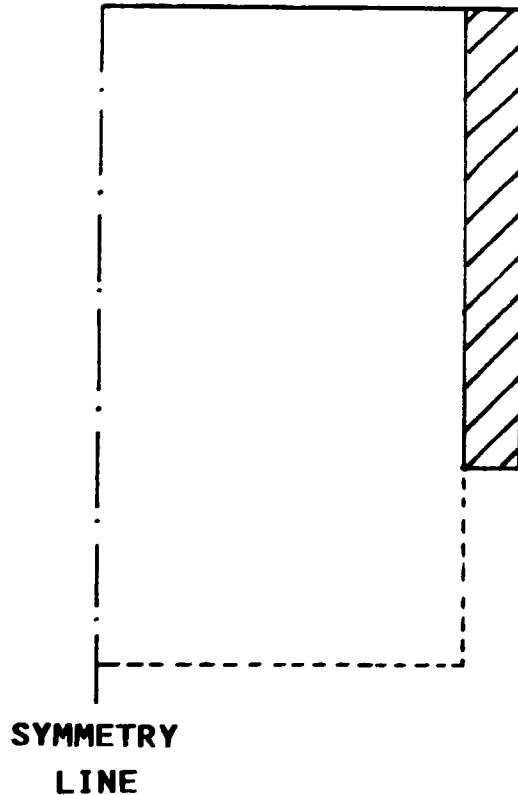
LINE DIAGRAM OF SINGLE-STRUT, REVERSE-SWEEP INLET

The first configuration is a single-strut, reverse-sweep inlet shown here in a line diagram. It has wedge-shaped sidewalls which are swept back at an angle of 30°. A compression strut is located in the center passage of the inlet, which is also swept, but it is swept forward at an angle of 30°. The throat width is held constant at all heights in the inlet, which results in an unswept throat. The cowl closure starts at D. Various other geometrical parameters are shown on the line diagram. Flow is calculated at the following conditions:

$$M_1 = 4.03, \quad P_1 = 8724 \text{ N/m}^2, \quad T_1 = 65°\text{K}$$

These correspond to experimental conditions.

$$H_1 = 2.75 \text{ in.}, \quad W = 1.005 \text{ in.}, \quad W/G = 4.16, \quad \delta_s = 6°$$

Section at DD'

Plane AA'
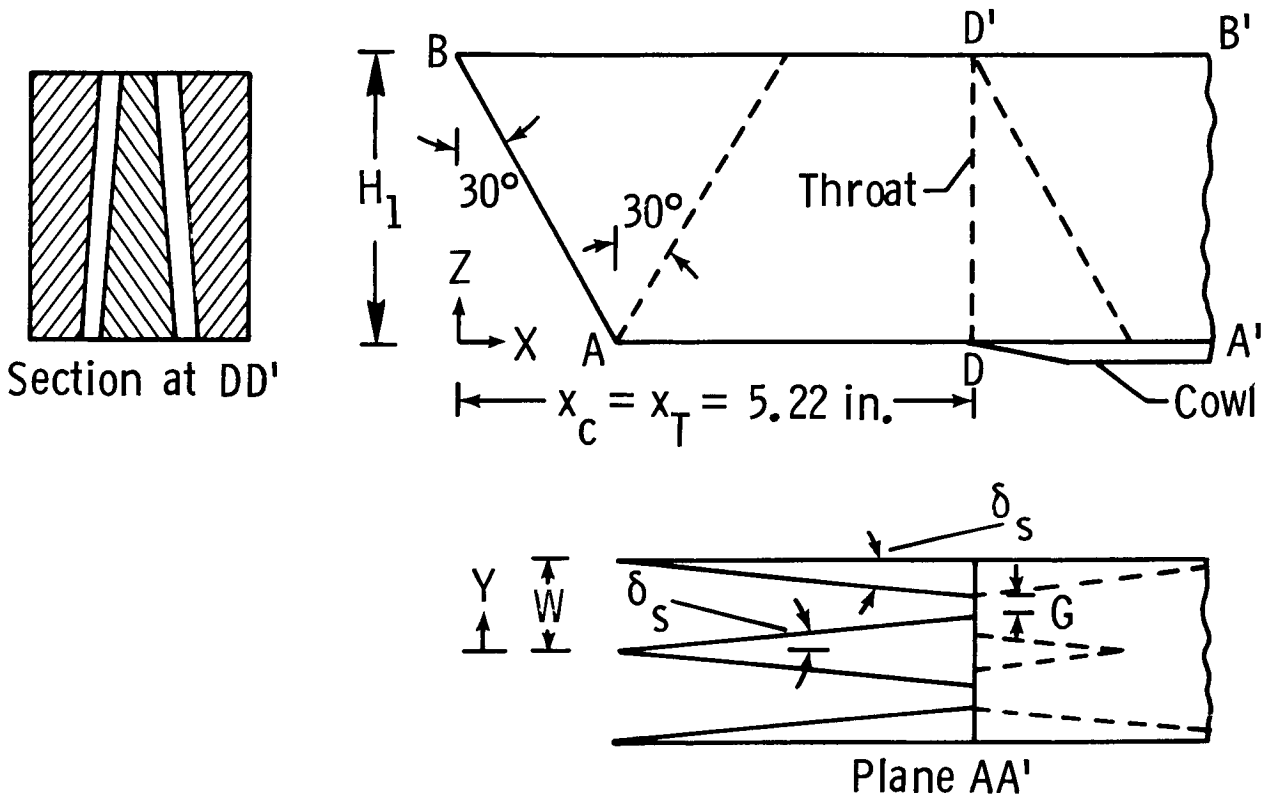
PRESSURE CONTOURS IN PLANES PARALLEL TO THE COWL PLANE

$$(M_1 = 4.03)$$

This figure shows the pressure contours in three planes corresponding to $z/H_1 = 0.145$, 0.5, and 0.89. One of the problems associated with single-strut inlets with similar sweep on the sidewalls and the strut is that for a given Mach number, the shock waves from the sidewalls and the strut will coalesce into a stronger shock wave which is not desireable for the operation of the inlet over a Mach number range with fixed geometry. In the present configuration, it appears that the shock wave coalescence problem is alleviated. Due to the opposite sweep, shock waves coalesce only in certain planes but not all across the inlet height at a given Mach number. For example, the pressure contours show that for the present conditions, shock waves coalesce in the planes near the top surface but not in the planes near the cowl.

$z/H_1 = 0.89$

$z/H_1 = 0.5$

$z/H_1 = 0.145$
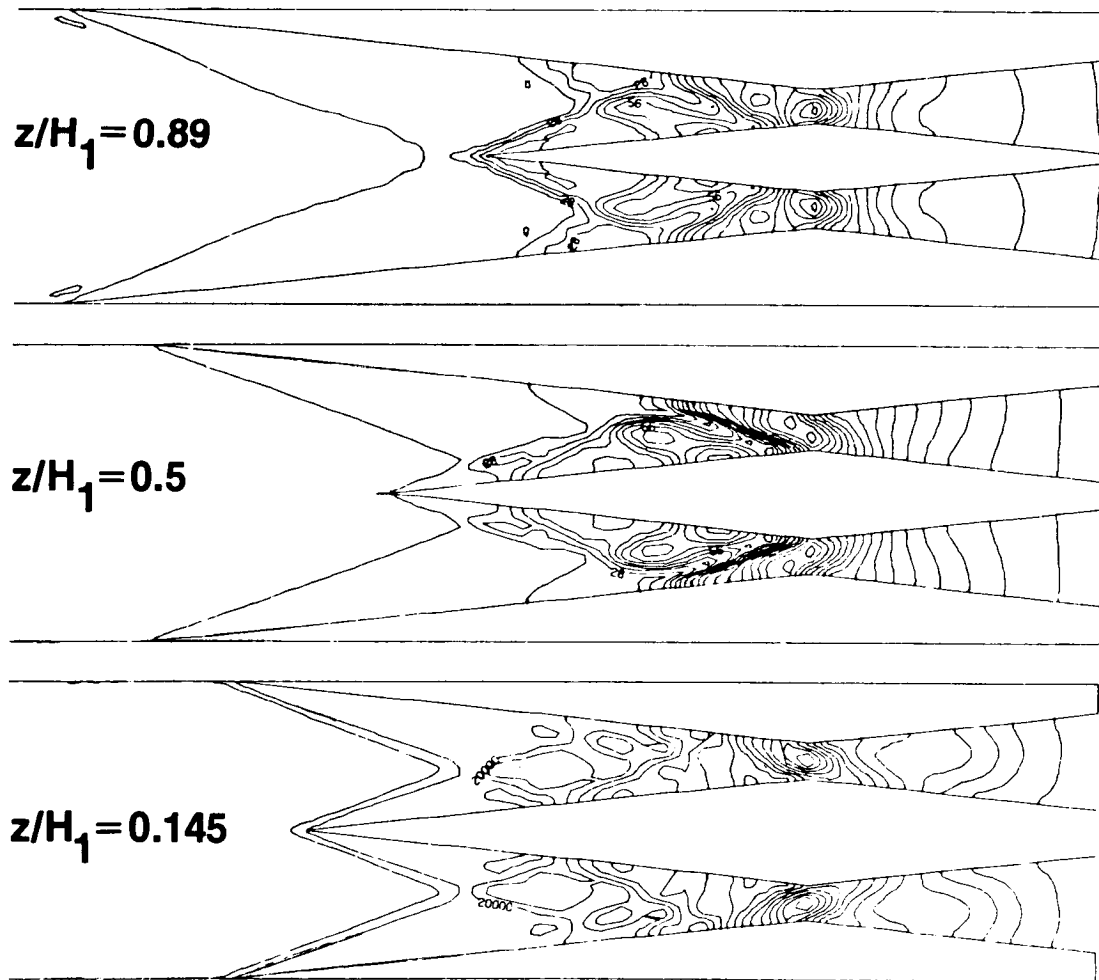
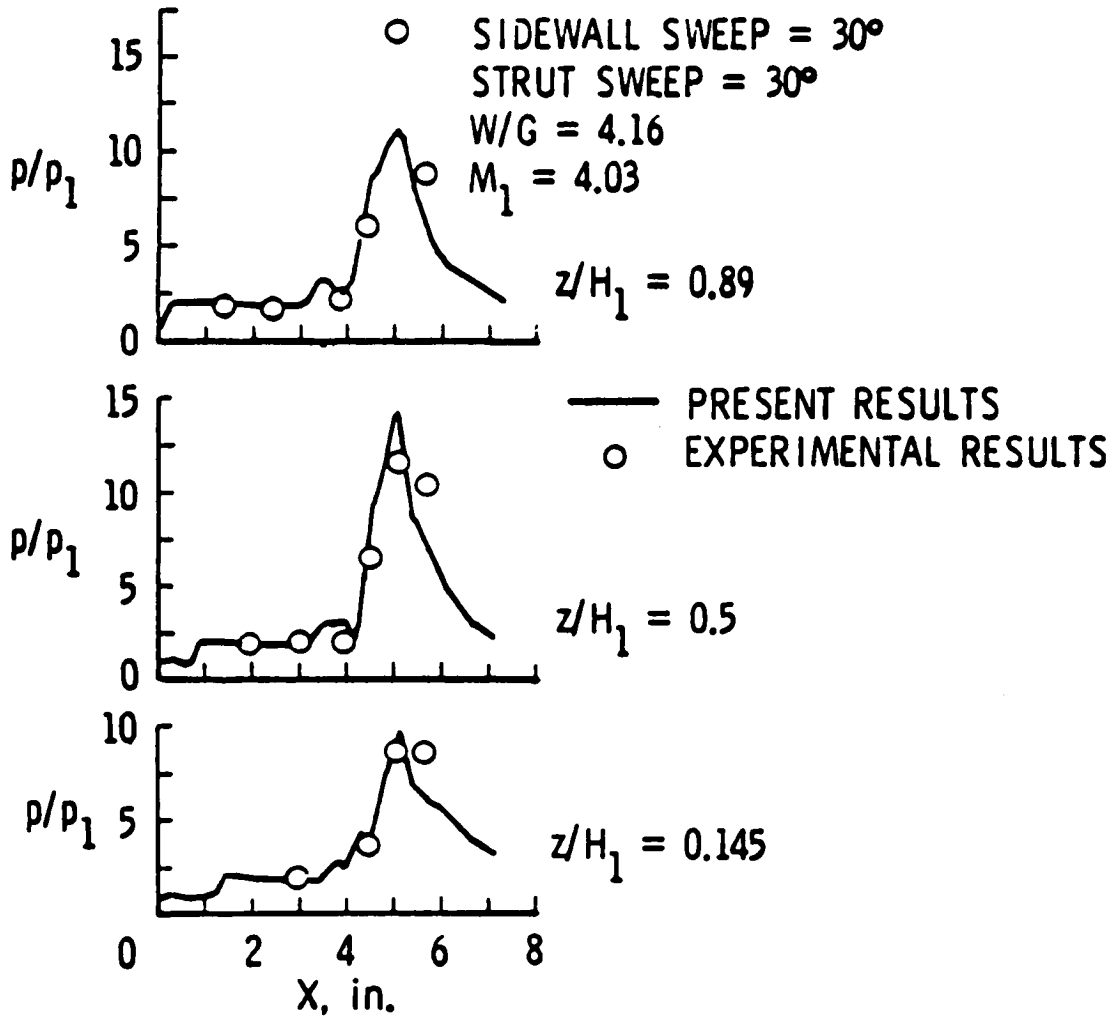# VELOCITY VECTOR FIELD IN PLANES PARALLEL TO THE COWL PLANE
$(M_1 = 4.03)$

This figure shows the velocity vector field in the same three planes. The separated flow regions on the sidewalls substantiate the observation made from the pressure contours.

z/H_1

0.89

0.5

0.145
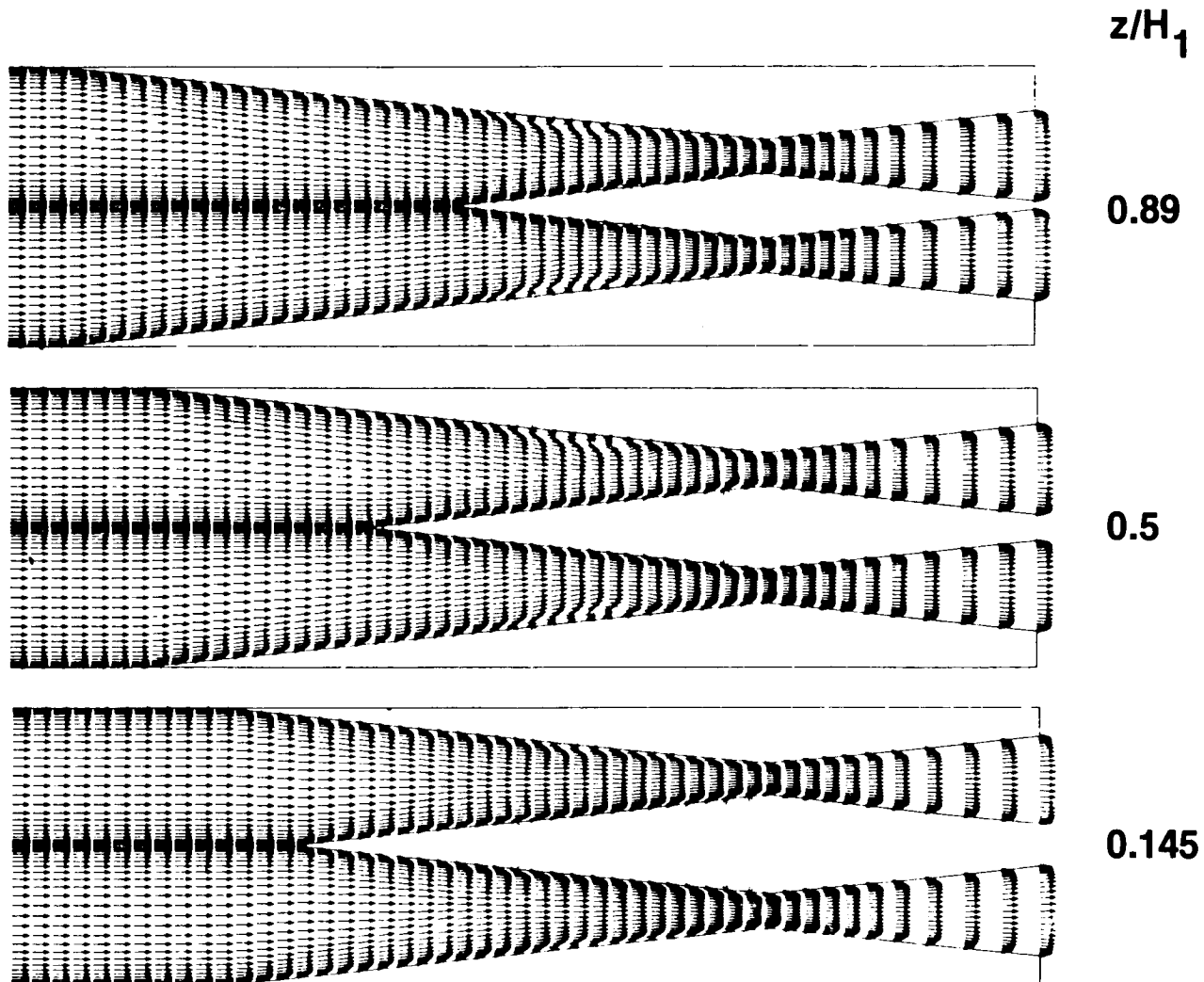
SIDEWALL PRESSURE DISTRIBUTIONS

This figure shows a comparison of the static sidewall pressure distributions with the experiment. It is seen that the predicted pressure levels compare very well with the experimental results up to the inlet throat. Deviations seen downstream of the throat are due to the fact that the experimental model had significantly different geometry than that used in the present calculations.

SIDEWALL SWEEP = 30°
STRUT SWEEP = 30°
W/G = 4.16
M_1 = 4.03

z/H_1 = 0.89

—— PRESENT RESULTS
O   EXPERIMENTAL RESULTS

z/H_1 = 0.5

z/H_1 = 0.145

X, in.

LINE DIAGRAM OF TWO-STRUT INLET

The second configuration for which results are presented here is a two-strut scramjet inlet. A line diagram of the inlet is shown below. This inlet also has wedge-shaped sidewalls which are swept back at an angle of 30°. Two compression struts are located in the center passage of the inlet and are also swept back at an angle of 30°. Sweep of all compression surfaces ends along line EF and the cowl closure starts at F. Various other geometrical parameters are shown on the line diagram. Flow is again calculated at Mach 4.03 in order to be able to compare with the experimental results.


Section along ZZ'

Plane AA'

Plane BB'
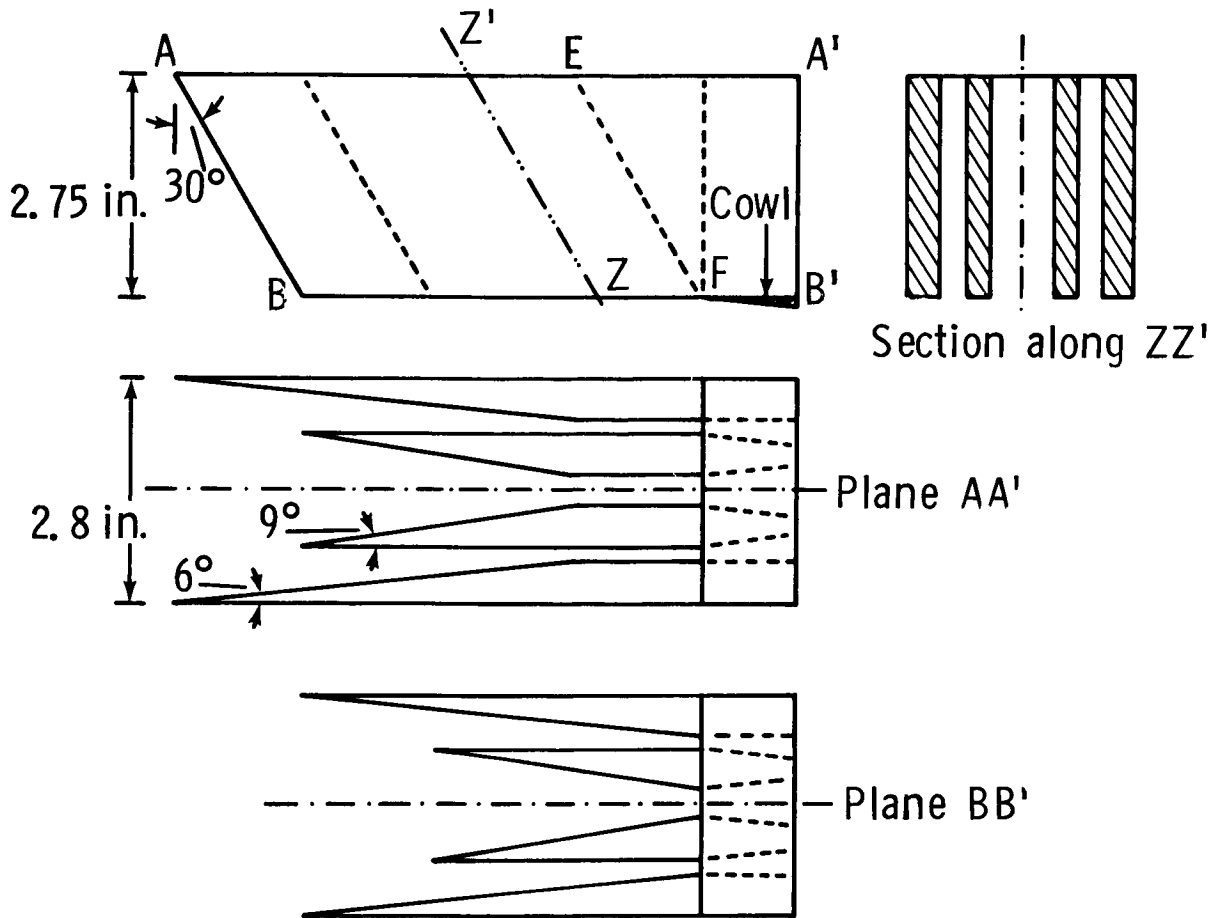
This figure shows the computational grid in one of the cross planes and in the symmetry plane. The calculations presented here are made with a grid of 41 x 51 x 37 points in x, y , z-directions, respectively. Out of the 37 planes in the z-direction, 11 planes lie under the cowl plane to account for the interaction between the internal and external flow.
Discretization of this inlet is further complicated by the struts embedded in the flow field. In order to accommodate the strut, the present analysis makes the strut surfaces coincident with two grid planes in the y-direction and further allows 10 more grid planes to go through the strut. This results in slight blunting of the strut leading edge, but this blunting is relatively small due to grid concentration in the neighborhood of the strut surfaces. A typical cross-plane grid is shown in the figure. If a particular cross plane lies above the cowl plane, the grid points lying within the strut are disregarded and proper boundary conditions are applied on the strut surfaces, but if the cross plane lies below the cowl plane, all grid points in the plane are used in the calculations.
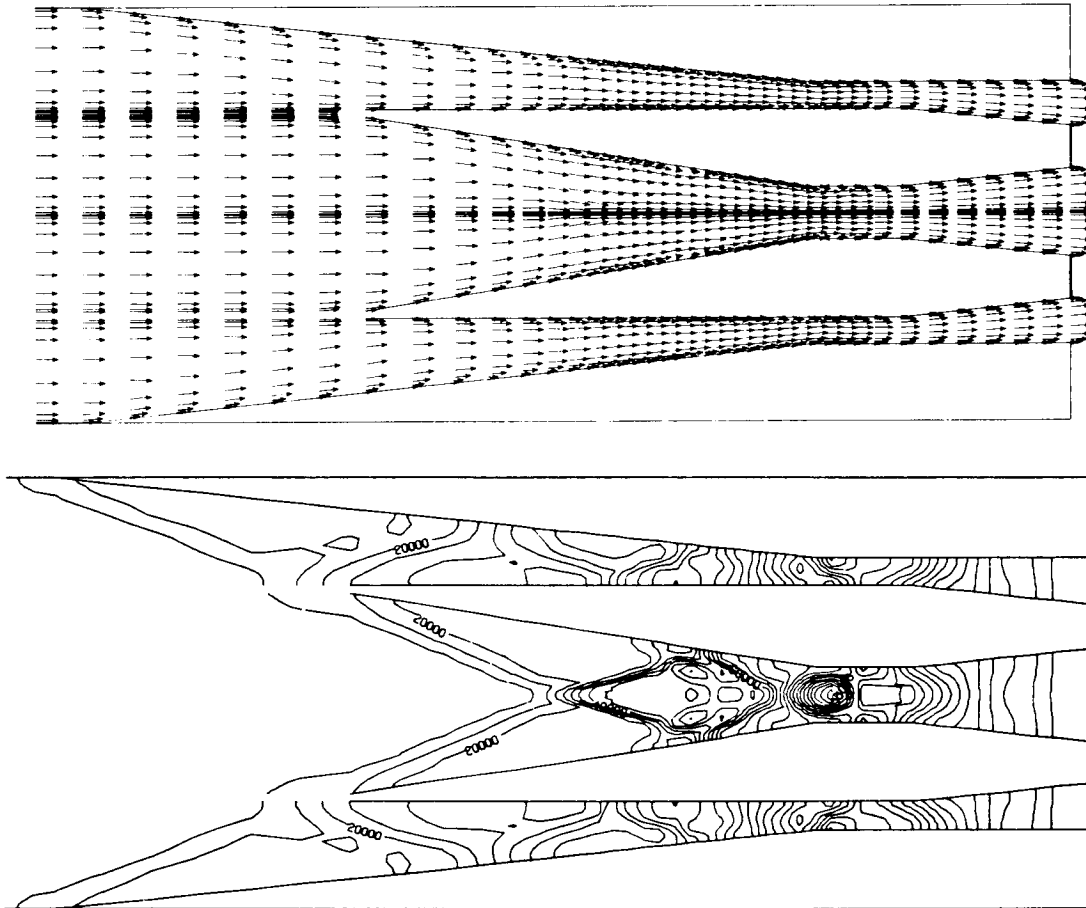
Symmetry plane
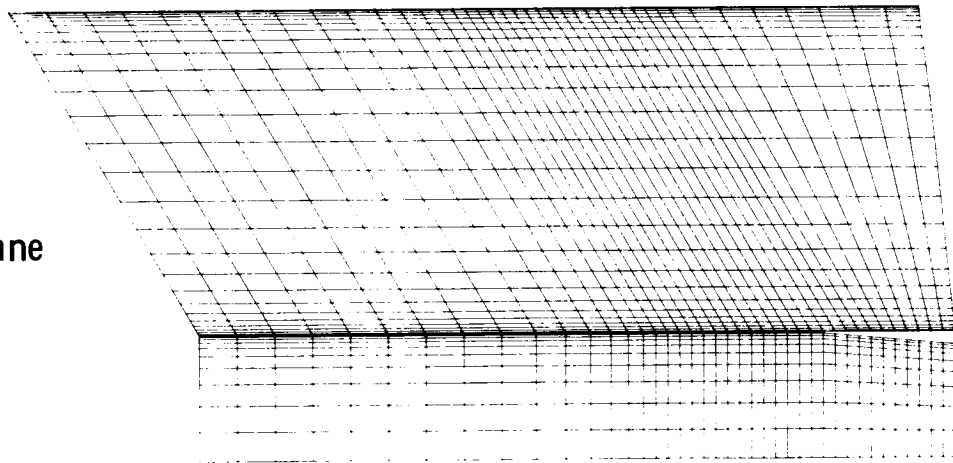
Cross plane
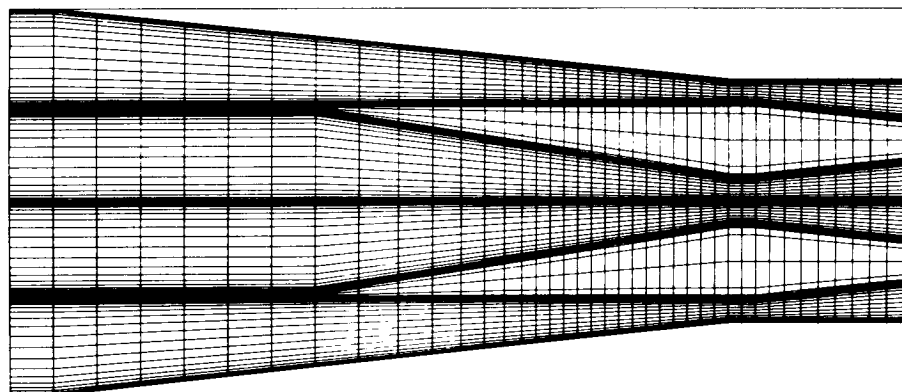
VELOCITY VECTOR FIELD AND PRESSURE CONTOURS IN PLANE LOCATED
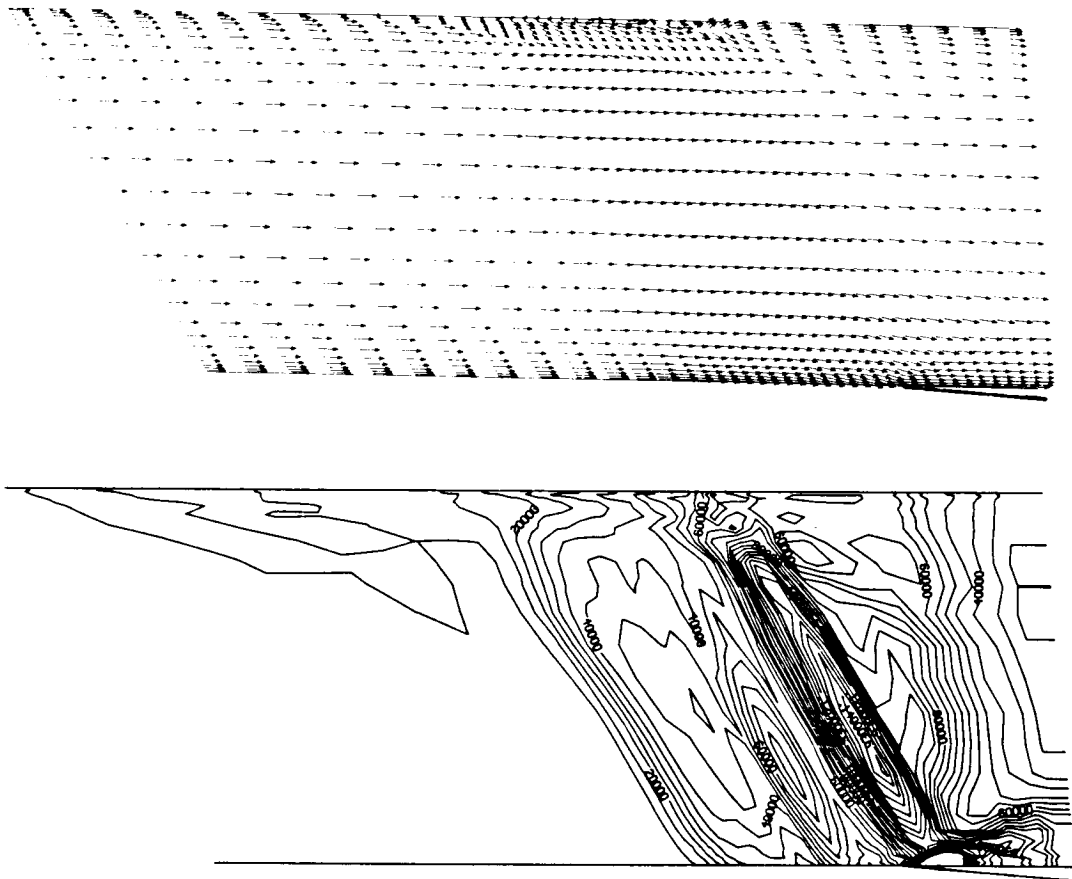
AT MID-INLET HEIGHT

This figure shows the velocity vector field and static pressure contours in a plane located at mid-inlet height. Slight blunting of strut leading edges and associated small distortions are obvious from this figure. The velocity vector plot shows several regions of separated flow caused by the shock/boundary-layer interaction and the pressure contour plot shows clearly the shock and expansion waves and their interactions.

203

VELOCITY VECTOR FIELD AND PRESSURE CONTOURS

IN THE SYMMETRY PLANE

This figure shows the velocity vector field and static pressure contours in the symmetry plane. The velocity vector field shows a downturn in flow direction ahead of cowl resulting in some flow spillage. The downturn is caused by the sidewall sweep and the interaction between the flow inside and outside of the inlet. Once the inlet flow passes behind the cowl leading edge, it is turned back parallel to the cowl plane, and this turning results in a cowl shock which can be seen in the pressure contour plot on this figure.
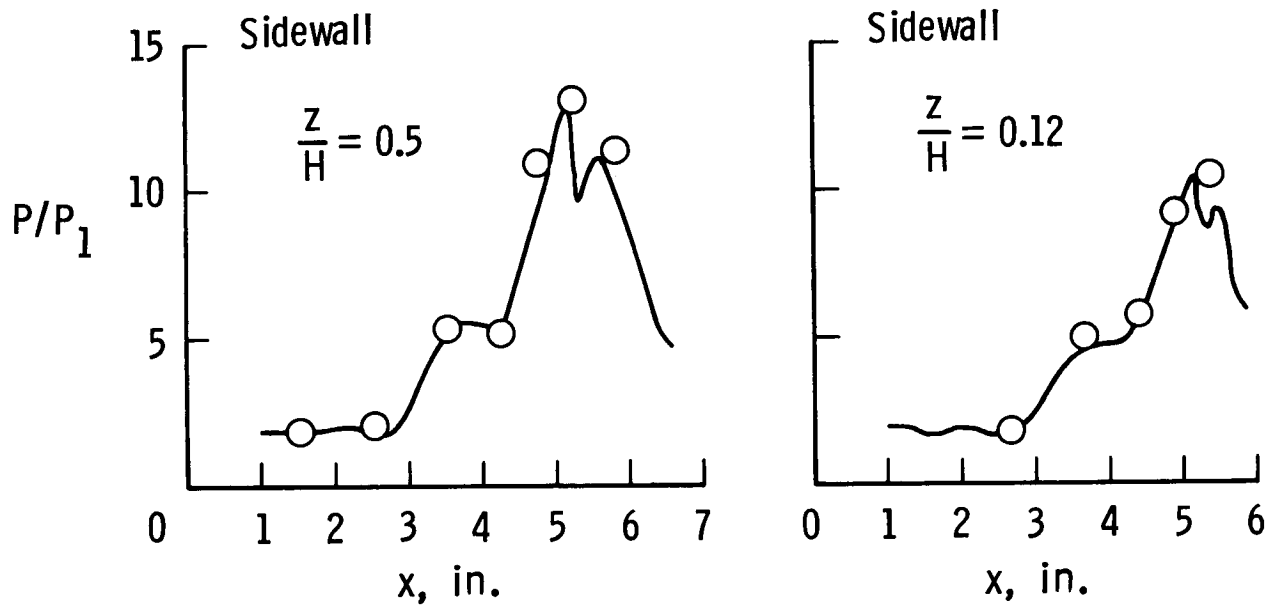
SURFACE PRESSURE DISTRIBUTIONS IN A TWO-STRUT SCRAMJET INLET

Static pressure distributions on the sidewall at two inlet heights are shown in this figure. As seen from the figure, the predicted pressure distributions compare very well with the experimental data.

—— Present results
O Experimental results (Trexler)

SURFACE PRESSURE DISTRIBUTION IN A TWO-STRUT SCRAMJET INLET

This figure shows a comparison of the predicted static pressure distribution with the experiment on the strut inner surface at mid-inlet height. Here again, the predicted results compare very well with the experiment.

Although not discussed much here, the flow captured by the inlet is an important measure of inlet performance. An accurate prediction of inlet capture also provides support to the procedure used here to account for the interaction between the internal and external flow ahead of the cowl. In the present analysis of the two configurations discussed here, predicted inlet flow capture compared very well with the experimentally predicted value.

Strut (Center Passage)
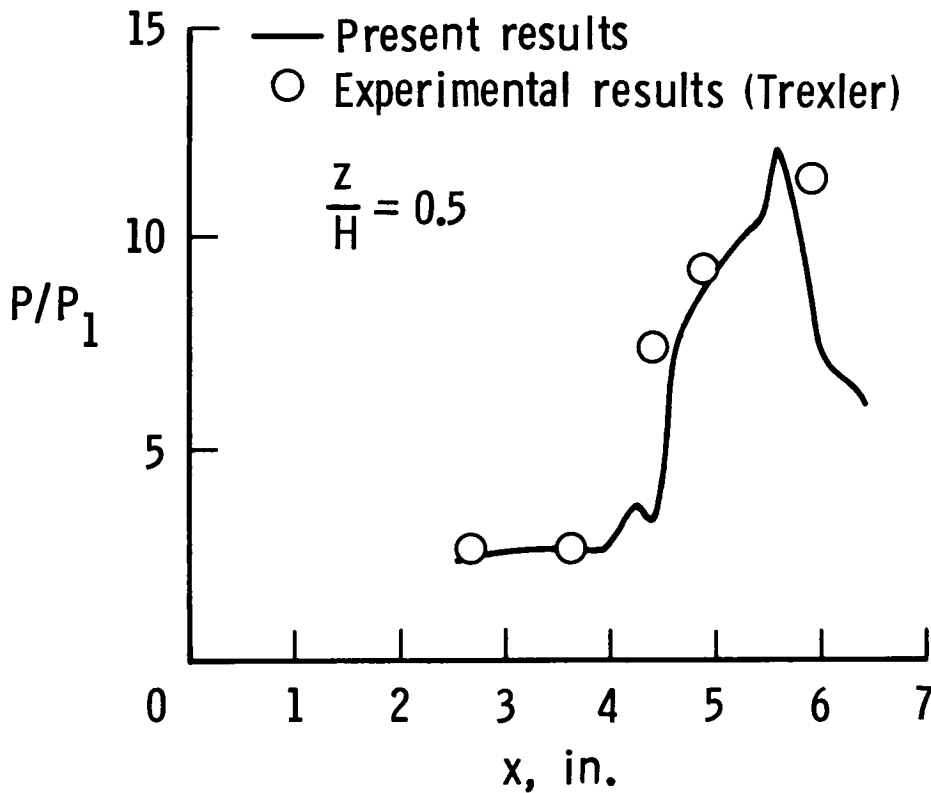
CONCLUDING REMARKS

- A series of inlet analysis codes (2-D, axisymmetric, 3-D) have been developed which can analyze complicated flow through complex inlet geometries in reasonably efficient manner

- The codes have been verified and are being used extensively to analyze practical inlet geometries both at Langley as well as industries

- Newly installed VPS 32 computer will allow more complex configurations to be analyzed

- Scalar Fortran versions available to increase transportability of the codes for use on other Scalar computers and on Cray vector processing computer

REFERENCES

1. Kumar, Ajay: Numerical Analysis of a Scramjet Inlet Flow Field Using the Three-Dimensional Navier-Stokes Equations. CPIA Publication 373, Feb. 1983, pp. 25-39.

2. West, J. E.; and Korkegi, R. H.: Supersonic Interaction in the Corner of Intersecting Wedges at High Reynolds Numbers. AIAA Journal, vol. 10, no. 5, May 1972, pp. 652-656.